Journal of Power Sources 206 (2012) 14–19

Contents lists available at SciVerse ScienceDirect

Journal of Power Sources

journal homepage: www.elsevier.com/locate/jpowsour

A non-precious metal bifunctional oxygen electrode for alkaline anion exchange membrane cells

Xu Wu, Keith Scott*

School of Chemical Engineering and Advanced Materials, Newcastle University, Newcastle upon Tyne, NE1 7RU, United Kingdom

ARTICLE INFO

Article history:
Received 31 October 2011
Received in revised form 3 December 2011
Accepted 26 December 2011
Available online 2 February 2012

Keywords:
Bifunctional oxygen electrode
Oxygen reduction reaction
Oxygen evolution reaction
Regenerative fuel cells
Electrolysis
Alkaline anion exchange membrane

ABSTRACT

An initial study of a non-precious metal based bifunctional oxygen electrode for use in regenerative fuel cells with alkaline anion exchange membranes is described. Four nanometer size $Cu_xMn_{0.9-x}Co_{2.1}O_4$ samples ($x = 0, 0.3, 0.6$, and 0.9) were prepared and characterized with XRD, SEM, TEM, and cyclic voltammetry. The $Cu_xMn_{0.9-x}Co_{2.1}O_4$ samples exhibited promising ORR and OER catalytic activities. The gap between ORR half wave potentials of Pt/C and $Cu_xMn_{0.9-x}Co_{2.1}O_4$ in 1 M KOH achieved only 50 mV. The onset potentials for OER on $Cu_xMn_{0.9-x}Co_{2.1}O_4$ catalysts were more than 100 mV more negative than Pt/C in 1 M KOH. MEA with $Cu_xMn_{0.9-x}Co_{2.1}O_4$ bifunctional oxygen electrode was prepared with CCM method and applied in a laboratory scale regenerative fuel cell. In fuel cell mode the peak power density was over 80 mW cm^{-2} and in electrolyser mode the onset voltage was about 1.55 V. The fuel cell to electrolyser voltage ration at 100 mA cm^{-2} achieved c.a. 31.87%.

1. Introduction

In the hydrogen energy system, water electrolysers and fuel cells are important electrochemical energy conversion devices. Water electrolysers may efficiently convert electricity from renewable power sources, such as solar, wind, and hydroelectric powers, into chemical energy with hydrogen as the energy carrier. The hydrogen fuel can be stored and transported, and utilized in combustion engines and fuel cells. Especially in H_2—O_2 fuel cells, the chemical energy carried by hydrogen can be efficiently released to electricity without burning, with large power densities suitable for vehicle and stationary use, of which the only byproduct is water. If the oxygen electrode exhibits catalytic activities for both oxygen reduction reaction (ORR) and oxygen evolution reaction (OER), it is possible to use one cell as either a fuel cell or electrolyser. In this way the two devices may be unitized to one, i.e. a regenerative H_2—O_2 fuel cell [1,2]. With suitable hydrogen and oxygen storages an efficient rechargeable H_2—O_2 battery could potentially be realized. The concept of a bifunctional oxygen electrode is also used in the operation of metal–air batteries [3]. An interesting feature of the conceptual rechargeable H_2—O_2 battery is that it avoids any CO_2 in the AAEM fuel cell system. In principle such rechargeable H_2—O_2 batteries may exhibit current densities (and thus output power) as large as that of polymer electrolyte fuel cells. The battery charging process of this H_2—O_2 battery will also be fast because of the large current densities used in the water electrolyser mode.

In previous unitized regenerative fuel cells, such a bifunctional oxygen electrode has often been based on mixed noble metal catalysts, typically a mixture of Pt and IrO_2, incorporated with perfluorinated sulphonic acid membranes (i.e. Nafion® developed by Dupont Ltd.) [4]. However, the costs of these precious metals are high for large scale applications. In a basic environment, the bifunctional oxygen catalysts can be made from none-precious-metal materials, such as first row spinel oxides and perovskite metal oxides [5], which are not suitable for Nafion-based regenerative fuel cells due to the acidity of the membrane. Due to recent developments of alkaline anion exchange membranes (AAEM) [6], application of none-noble-metal bifunctional oxygen electrode becomes of potential interests [2].

Previous reviews have identified spinel oxides, based on cobaltite, as potential bifunctional catalysts for high pH operation [7]. Rios et al. [8] found that the $Mn_xCo_{3-x}O_4$ mixed valency spinel oxides exhibits both OER and ORR catalytic activities and although the Mn content catalyzed the ORR it inhibited the OER. Other investigations also suggested that MnO_x was a promising bifunctional catalysts [2,9]. Cheng and co-workers [10] prepared nano-crystalline spinels of $Co_xMn_{3-x}O_4$ using a rapid room-temperature synthesis method and found that $Co_xMn_{3-x}O_4$ nanoparticles exhibited considerable OER and ORR catalytic activities due to their high surface areas and abundant defects. $Cu_xCo_{3-x}O_4$ was also suggested a promising bifunctional catalyst [11]. Later, De Koninck and Marsan proposed a Mn-doped

* Corresponding author. Tel.: +44 191 2225207; fax: +44 191 2225292.
E-mail address: k.scott@ncl.ac.uk (K. Scott).

0378-7753/$ – see front matter © 2011 Elsevier B.V. All rights reserved.
doi:10.1016/j.jpowsour.2011.12.052

$CuCo_2O_4$ [12] to improve electrocatalytic activities of the Cu doped cobaltite oxides. In their studies poly(vinylidene fluoride-co-hexafluoropropylene) was used as a binder for the catalyst layer/film. To improve activity in practical electrodes, seeking suitable ionomers is an important step for developing high performance MEAs of fuel cells and electrolysers [13–15]. In previous work we have used a developmental ionomer, which has quaternary ammonium hydroxyl conducting groups and perfluorinated hydrophobic groups, with $Cu_xCo_{3-x}O_4$ catalysts for alkaline anion exchange membrane water electrolysers [13]. Besides, in our previous studies cobalt-based ORR catalysts have demonstrated high and stable power density performances (>200 mW cm^{-2}) in practical AAEM fuel cells [14]. In this study, the Mn and Cu incorporated Co_3O_4 nanometer-size powders were prepared with a thermal decomposition method and characterized with SEM, TEM, and XRD. Its catalytic activities for OER and ORR were studied with cyclic voltammetry. A membrane electrode assembly (MEA) for regenerative H_2—O_2 fuel cell was prepared using this non-precious metal catalyst in the bifunctional oxygen electrode and with an alkaline anion exchange membrane, and its performances in water electrolyser mode and in fuel cell mode were determined with linear sweep voltammetry and impedance spectroscopy.

2. Experimental methods

2.1. Configuration

A laboratory scale regenerative H_2—O_2 fuel cell is schematically illustrated in Fig. 1. At the heart of this regenerative fuel cell is the MEA, on each side of which are respectively the oxygen electrode and hydrogen electrode. In this cell only deionized water is used, without any electrolytes such as KOH. The tanks were firstly filled with deionized water. Water from the water tanks is pumped through the cell and recirculated back to the water tanks. With electricity from external power sources, hydrogen and oxygen gases are generated on corresponding electrode via water electrolysis. Then H_2 and O_2 gases could be collected by removable storage segments. Actually, the two gas products may be transferred to and consumed by other devices like combustion engines and fuel cells. As a unitized regenerative fuel cell, the H_2 and O_2 gases can be supplied to the MEA of the system to operate in the fuel cell mode as shown in Fig. 1, to produce electricity at the MEA. In this process the only byproduct is H_2O, which can flow back to the water tanks. Carefully sealing certain amount of deionized water and improving segments of this system may possibly make it a stand alone regenerative fuel cell, which would function as a rechargeable H_2—O_2 battery. An interesting advantage of the conceptual rechargeable H_2—O_2 battery is that this design may easily avoid any CO_2 in the AAEM fuel cell system. Such rechargeable H_2—O_2 batteries may exhibit current densities (and thus output power) as large as that of polymer electrolyte fuel cells. More importantly, the battery charging process (i.e. the water electrolysis process) of this H_2—O_2 battery will be remarkably fast because of large current densities when the MEA works in water electrolyser mode. On the other hand, in term of storing energy from external power sources, the production of H_2 and O_2 is mainly limited by the amount of supplied water. As well, the quantity of electricity generated by the regenerative fuel cell could be long-playing with sufficient H_2 and O_2.

2.2. Materials preparation

The Cu and Mn incorporated Co_3O_4 nanoparticles were prepared with a sodium nitrate thermal treatment method, which is similar with the method we reported on preparing Cu incorporated Co_3O_4 catalysts [13]. In this method, excessive $NaNO_3$ (stoichiometrically at least 50 times more than metal) was added into a solution of $CuCl_2{\cdot}2H_2O$, $MnCl_2{\cdot}4H_2O$, and $CoCl_2{\cdot}6H_2O$ (Sigma Aldrich) in deionized water and ethanol (with volume ratio water:ethanol = 1:4, and with a total metal concentration of 0.1–0.2 mol dm^{-3}) when the solution was being stirred. The slurry mixture was dried at 70 °C over night and consequently calcined in air at 400–500 °C for 2–3 h, depending on the amount of precursors. The particles of the oxides may be controlled to nanometer size by the dispersion effect of excess $NaNO_3$. After heat-treatment, the sample was rinsed with de-ionized water and centrifuged to remove any soluble contents. Finally, the oxide was dried at 70 °C in air before storage. Four $Cu_xMn_{0.9-x}Co_{2.1}O_4$ samples were prepared and studied in this study, of which the x values were respectively 0, 0.3, 0.6, and 0.9.

The AAEM adopted in this study is prepared with the method similar with that described in our previous publications [14]. The membrane was prepared by radiation grafting with γ-radiation source consists of 20 rods of Cobalt-60 encapsulated in steel tubes in an open cylindrical arrangement. Typical source activity is 146 Tera Bequerels (TBq), with a maximum dose rate of 12.74 kGy h^{-1}. Pieces of the polymer were interleaved with a non-woven material and then placed in a grafting tube, which was filled with the monomer solution until the complete roll was saturated and covered. Then, the vessel was purged with nitrogen gas to remove oxygen. The irradiation was lasted for a pre-determined time at a known dose rate at 23 ± 1 °C. After radiation grafting, the polymer was washed with toluene and dried to constant weight in an oven at 70 °C. The conductivity of this membrane was found between 0.04 and 0.076 S cm^{-1} in the temperature range 20–60 °C.

The MEA was prepared with a catalysts coated membrane (CCM) method similar with reported fabrication method [15]. Catalyst inks containing deionized water, ethanol, support, and a developmental ionomer were prepared with ultrasonic mixing. The oxygen electrode, which contains 3 mg cm^{-2} $Cu_xMn_{0.9-x}Co_{2.1}O_4$, and hydrogen electrode (50 wt.% Pt/C, Alfa Aesar, loading 1 mg Pt cm^{-2}) were coated onto opposite sides of the membrane using an air-brush with 2 bar nitrogen gas. Before MEA fabrication, the membrane was thoroughly rinsed with deionized water. After fabrication, the MEAs were immersed in a 1 mol dm^{-3} KOH solution to completely convert the membrane from Cl^- to OH^- form (the solution will be changed several times during immersion), and then rinsed several times with excess deionized water until none Cl^- was detected in the rinsing water.

2.3. Characterizations

The $Cu_xMn_{0.9-x}Co_{2.1}O_4$ samples (x = 0, 0.3, 0.6, and 0.9) were characterized with X-ray diffraction (XRD, PANalytical X'Pert Pro Diffractometer, with Cu Kα radiation of wavelength 0.15406 nm), transmission electron microscope (TEM, Philips CM100), and scanning electron microscopy (SEM, JEOL JSM5300LV).

Electrochemical experiments were carried out in a 3-electrode glass cell in 1 mol dm^{-3} KOH solution prepared with deionized water. A Hg/HgO in 1 mol dm^{-3} KOH reference electrode (+0.0977 V vs. standard hydrogen electrode at 25 °C) was connected to a Luggin capillary which was positioned very close to the working electrode. The counter electrode was a Pt foil (1 cm × 2.5 cm). The working electrode was prepared by applying a drop the catalyst ink onto a rotating disc electrode (glassy carbon with geometric area 0.07069 cm^2) with a micropipette and drying beneath an infrared lamp for 10 min. Electrochemical measurements were performed with a Voltalab® potentiostat (Radiometer Voltalab PGZ100). Unless otherwise specified, all potentials in this paper were referred to the Hg/HgO electrode in 1 mol dm^{-3} KOH and the catalyst loading was always 100 μg cm^{-2}. Prior to measurement, the KOH solution was bubbled with either nitrogen or oxygen for

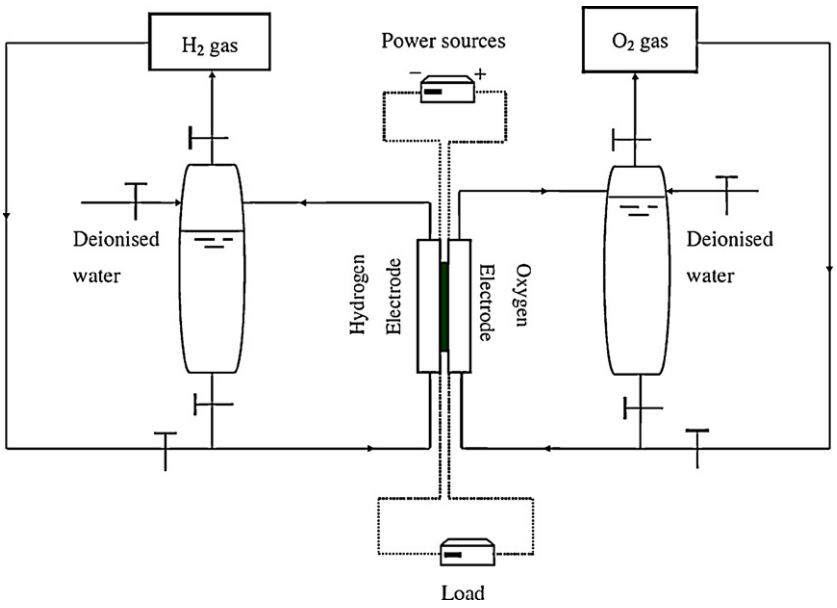

Fig. 1. Schematic figure of regenerative H_2—O_2 fuel cells experiments.

20 min for OER and ORR studies respectively. Linear sweep voltammograms (LSV) of half cell test were obtained with a scan rate of 10 mV s^{-1}.

In MEA tests two carbon papers (Toray, TGP-H-090) were pressed onto each side of the MEA and used as current connectors. When the MEA was installed in the testing system, the oxygen electrode side (shown in Fig. 1) was connected to potentiostat as working electrode and the hydrogen electrode side was adopted as a pseudo reference as well as counter electrode. The polarization curves of the practical MEA were obtained with a scan rate of 1 mV s^{-1}; this rate being sufficiently slow as to not introduce hysteresis in the backward and forward scans.

3. Results and discussion

3.1. XRD

Fig. 2 shows the X-ray powder diffraction patterns of $Cu_xMn_{0.9-x}Co_{2.1}O_4$ nanoparticles in a 2θ range 15–70°. All four samples exhibited diffraction patterns identical with spinel Co_3O_4 (JCPDS 00-042-1467), with a cubic lattice structure and space group Fd3m-227. There were no extra diffraction peaks in all cases, which might indicate that the $Cu_xMn_{0.9-x}Co_{2.1}O_4$ samples were solid solutions with simple spinel structure. Previous studies have also revealed that incorporation of foreign metals into the Co_3O_4 lattice may lead to a solid solution in the form $M_xCo_{3-x}O_4$ (M = Mn, Cu, etc.), when x was less than 1.0 [8,11–13]. The peaks of Mn incorporated samples were apparently broader and less sharp than those of the $Cu_{0.9}Mn_{0.0}Co_{2.1}O_4$ sample, which to some extent may indicate Mn is more effective for nanocrystallization of the cobaltite than Cu. With the d-spacing of (3 1 1) plane, crystallite sizes of the samples were calculated according to the Scherrer equation, the results approximately 19.0 nm, 10.8 nm, 13.2 nm, and 11.5 nm, for $Cu_{0.9}Mn_{0.0}Co_{2.1}O_4$, $Cu_{0.6}Mn_{0.3}Co_{2.1}O_4$, $Cu_{0.3}Mn_{0.6}Co_{2.1}O_4$, and $Cu_{0.0}Mn_{0.9}Co_{2.1}O_4$ respectively.

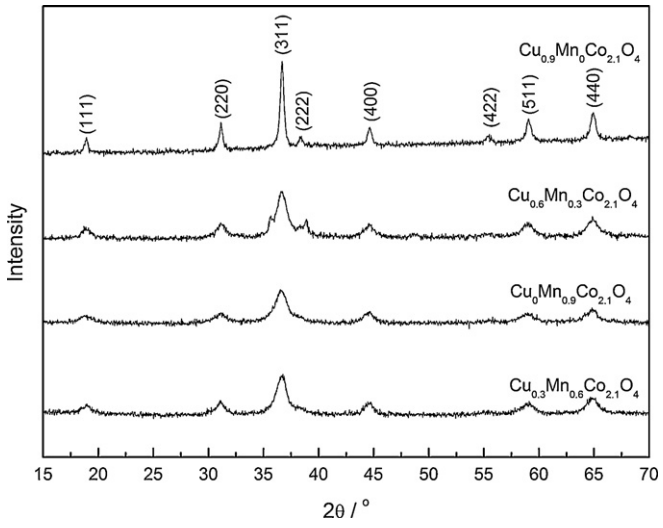

Fig. 2. XRD of $Cu_xMn_{0.9-x}Co_{2.1}O_4$ nanoparticles (x = 0, 0.3, 0.6, and 0.9).

3.2. Morphology of the catalysts

The particle sizes of $Cu_xMn_{0.9-x}Co_{2.1}O_4$ samples were also investigated from microscopy and data are shown in Fig. 3. In Fig. 3(A) the morphology of $Cu_{0.3}Mn_{0.6}Co_{2.1}O_4$ can be seen as small clusters of nanometer-size powders. When the nanopowders were finely dispersed, their morphology was clearer in TEM. The majority of $Cu_{0.3}Mn_{0.6}Co_{2.1}O_4$ nanopowders are cubic, with particle sizes of about 10–15 nm. Smaller particle sizes would lead to larger surface areas, which is beneficial for their catalytic activities. However, the crystallite size of cobaltite was found sensitive to the preparation processes, including treatment of precursors and calcination parameters [9]. In this study, the $Cu_xMn_{0.9-x}Co_{2.1}O_4$ samples of crystallite sizes 10–20 nm could be reproduced.

3.3. ORR activity

The activities for ORR of $Cu_xMn_{0.9-x}Co_{2.1}O_4$ and Pt/C catalysts were compared in the LSVs, shown in Fig. 4. The oxygen reduction onset potentials of $Cu_xMn_{0.9-x}Co_{2.1}O_4$ samples were slightly less positive than that of Pt/C. Amongst the four samples, the LSV of $Cu_{0.0}Mn_{0.9}Co_{2.1}O_4$ was the closest to that of Pt/C and $Cu_{0.9}Mn_{0.0}Co_{2.1}O_4$ exhibited the biggest difference. This result may indicate that Mn content has a positive influence on ORR activity of $Cu_xMn_{0.9-x}Co_{2.1}O_4$, which agrees with literature view [8,10,12,16]

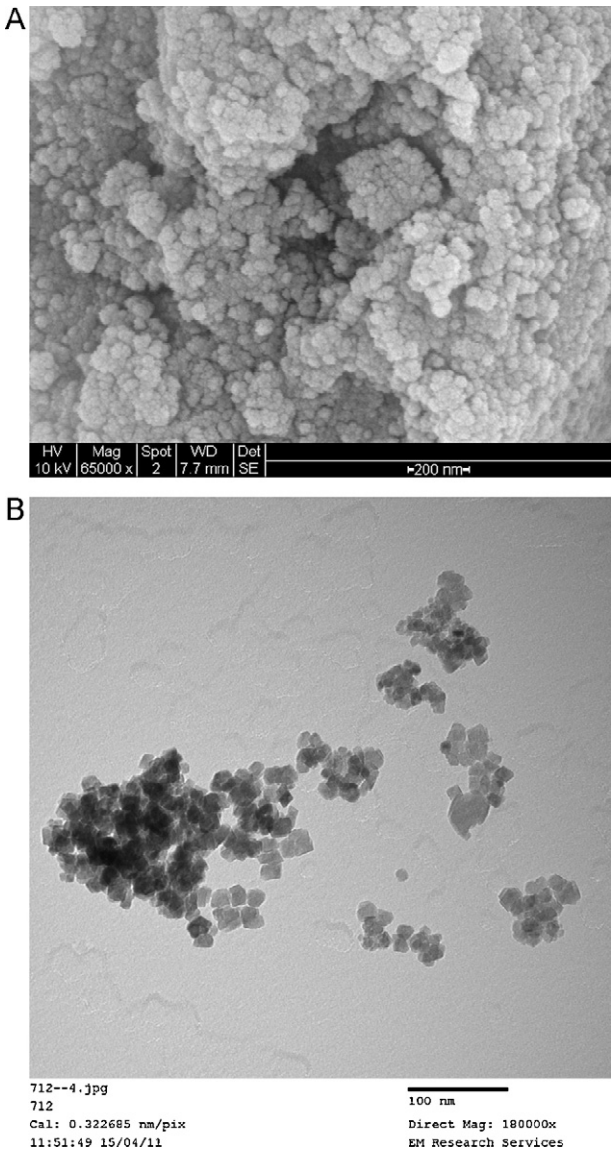

Fig. 3. Morphology of $Cu_{0.3}Mn_{0.6}Co_{2.1}O_4$ in (A) SEM and (B) TEM.

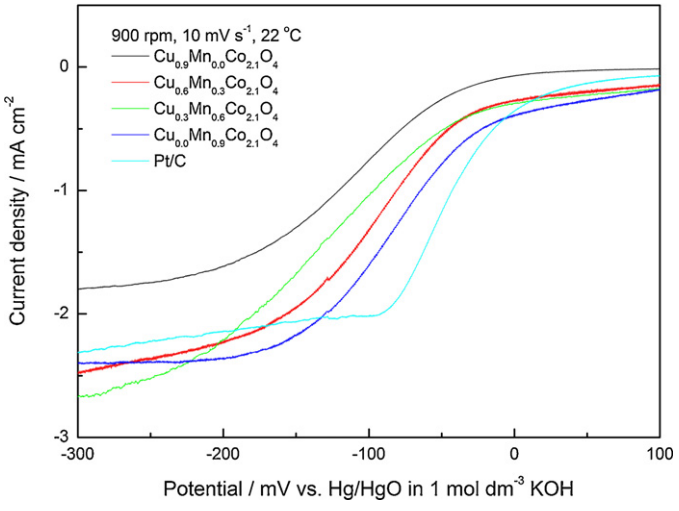

Fig. 4. LSVs of ORR on $Cu_xMn_{0.9-x}Co_{2.1}O_4$ and Pt/C in O_2 saturated 1 mol dm^{-3} KOH solution.

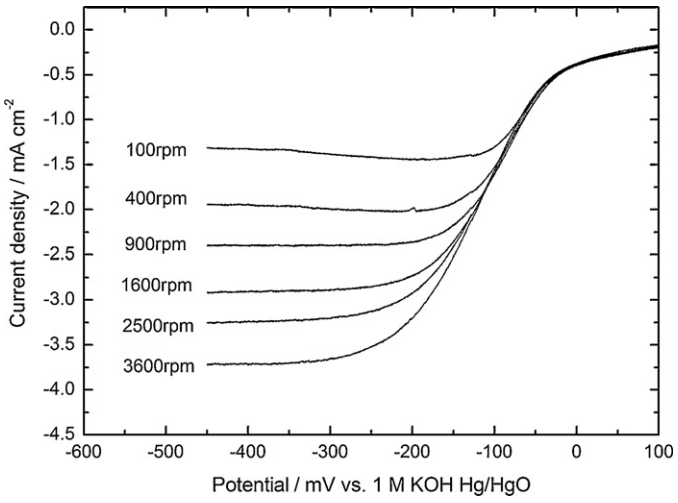

Fig. 5. LSVs of $Cu_{0.0}Mn_{0.9}Co_{2.1}O_4$ on RDE in O_2 saturated 1 mol dm^{-3} KOH at 20 °C with a sweep rate of 10 mV s^{-1}.

that Mn content in cobaltite oxide influences the ORR activity significantly. Pt/C is commonly considered the best catalyst for ORR in polymer electrolyte fuel cells. The difference between ORR half wave potentials of Pt/C and $Cu_{0.0}Mn_{0.9}Co_{2.1}O_4$ was less than 50 mV, which indicates good ORR catalytic activity of $Cu_xMn_{0.9-x}Co_{2.1}O_4$. Notably, the current density displayed by $Cu_{0.9}Mn_{0.0}Co_{2.1}O_4$ in Fig. 4 was smaller than other samples, which might be due to the particle size of $Cu_{0.9}Mn_{0.0}Co_{2.1}O_4$ is larger than others, as determined by XRD.

The kinetic parameters of oxygen reduction reaction on $Cu_xMn_{0.9-x}Co_{2.1}O_4$ catalyst were investigated with a rotating disc electrode (RDE). Fig. 5 shows typical ORR polarization curves of $Cu_{0.0}Mn_{0.9}Co_{2.1}O_4$ with rotation speeds 100–3600 rpm. According to the Koutecky–Levich law, the overall current at a given potential (I) is related to the angular rotation speed of RDE (ω, rad s^{-1}) according to:

$$\frac{1}{I} = \frac{1}{I_k} + \frac{1}{I_{dl}} \quad (1)$$

$$I_k = nFAkC_{O_2} \quad (2)$$

$$I_{dl} = 0.62nFAD_{O_2}^{2/3}\nu^{-1/6}C_{O_2}\omega^{1/2} = B\omega^{1/2} \quad (3)$$

$$\frac{1}{I} = \frac{1}{I_k} + \frac{1}{B} \times \omega^{-1/2} \quad (4)$$

where I_k and I_{dl} are respectively the kinetic current and diffusion limited current, n is number of electrons involved in the reduction process, F is the Faraday constant (96,485 C mol^{-1}), A is the electrode geometric area, k is the apparent rate constant for oxygen reduction, C_{O_2} is the concentration of O_2 in 1 mol dm^{-3} KOH solution at 25 °C (0.93×10^{-6} mol cm^{-3}), D_{O_2} is the diffusion coefficient of O_2 in 1 mol dm^{-3} KOH solution (1.76×10^{-5} cm^2 s^{-1}), ν is the kinetic viscosity of the solution at 25 °C (0.01 cm^2 s^{-1}).

Fig. 6 demonstrates the Koutecky–Levich plots at different potentials on $Cu_{0.0}Mn_{0.9}Co_{2.1}O_4$ electrode. All plots exhibited linear dependence, which commonly may indicate first-order kinetics with respect to oxygen. In alkaline media, the following two pathways are usually considered:

(i) Direct four electron pathway:

$$O_2\,(ads) + 2H_2O + 4e^- \leftrightarrow 4OH^- \quad (E_{rev} = 0.41 \text{ V at pH} = 14) \quad (5)$$

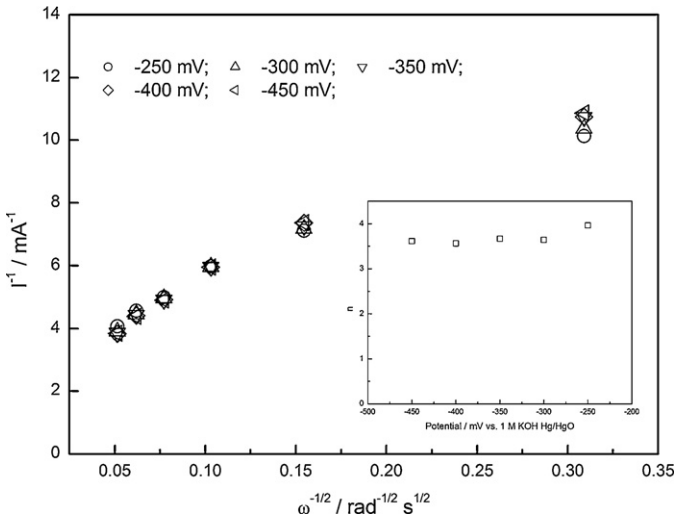

Fig. 6. Koutecky–Levich plots obtained from Fig. 5 at different potentials, insert figure is variation of *n* with potential.

(ii) Peroxide (indirect) pathway:

$$O_2\ (\text{ads}) + H_2O + 2e^- \leftrightarrow OH^- + HO_2^- \quad (E_{\text{rev}} = -0.065\ \text{V at pH} = 14) \tag{6}$$

followed by either the further reduction of peroxide ions:

$$HO_2^- + H_2O + 2e^- \rightarrow 3OH^- \quad (E_{\text{rev}} = 0.867\ \text{V at pH} = 14) \tag{7}$$

Or the catalytic peroxide decomposition:

$$HO_2^- \rightarrow (1/2)O_2 + OH^- \tag{8}$$

With the slopes of the plots in Fig. 6, the number of electrons transferred per oxygen molecule (n) for ORR on $Cu_{0.0}Mn_{0.9}Co_{2.1}O_4$ was determined and plotted in the insert figure. The n values in this study vary from 3.7 to 4 and agree with results of literature [8,16]. Results of Sugawara's study [16] on Mn—Co spinel oxides supported direct four electron reduction on this catalyst. It was argued by Rios et al. that the ORR on Mn incorporated cobaltite possibly follows the two "interactive" and "parallel" pathways [8].

3.4. OER activity

Fig. 7 shows anodic linear sweep voltammograms for the OER on the $Cu_xMn_{0.9-x}Co_{2.1}O_4$ and Pt/C catalysts. In the potential range 500–550 mV, all $Cu_xMn_{0.9-x}Co_{2.1}O_4$ samples exhibited anodic peaks typical of spinel cobaltite electrodes, which were followed by the onset points of oxygen evolution. The onset potential of OER on Pt/C was significantly more positive than $Cu_xMn_{0.9-x}Co_{2.1}O_4$ samples. $Cu_{0.6}Mn_{0.3}Co_{2.1}O_4$ sample exhibited the more negative potentials in the investigated current density range. Previous studies on $Cu_xCo_{3-x}O_4$ OER catalysts [13] suggested that the inversion of Cu^{2+} into octahedral sites and Co^{3+} to the tetrahedral sites may change the surface properties and therefore may lead to negative "shift" of OER on the cobaltite catalysts. Additional characterization techniques will be applied to study the surface properties of these catalysts in future works. It may be reasonable to consider that there would be an optimal composition of Cu and Mn incorporated spinel cobalt oxide in terms of OER catalytic activity.

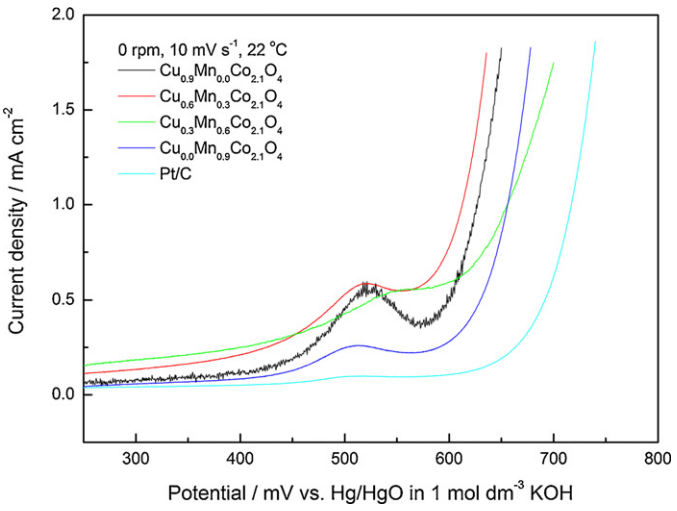

Fig. 7. LSVs of OER on $Cu_xMn_{0.9-x}Co_{2.1}O_4$ and Pt/C in 1 mol dm^{-3} KOH solution.

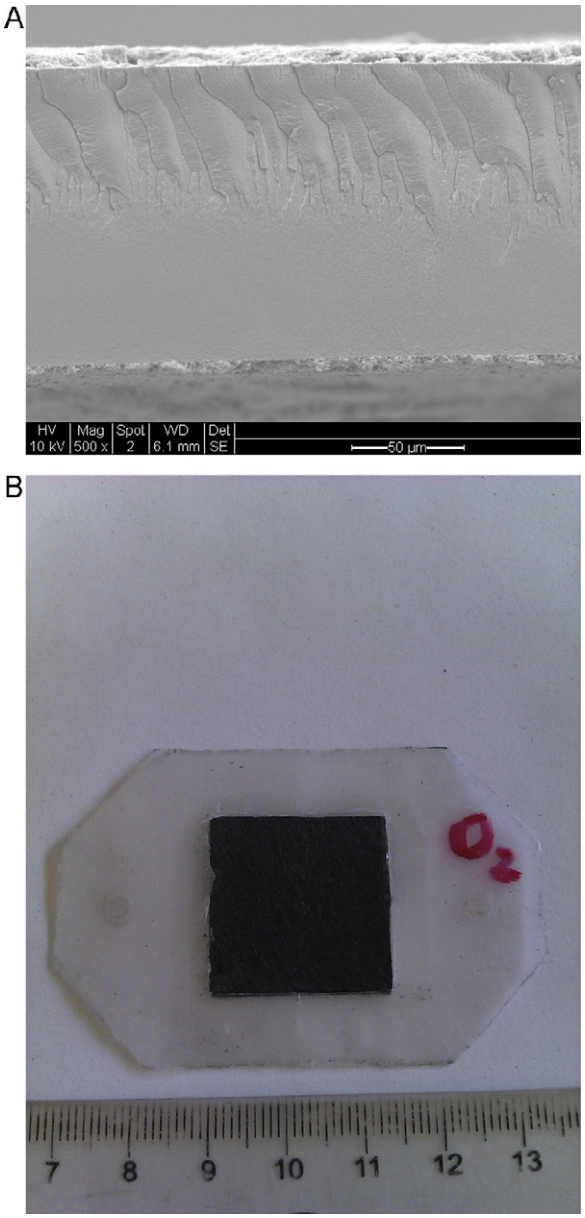

Fig. 8. MEA prepared with CCM method: (A) cross-section in SEM and (B) actual photo of final product.

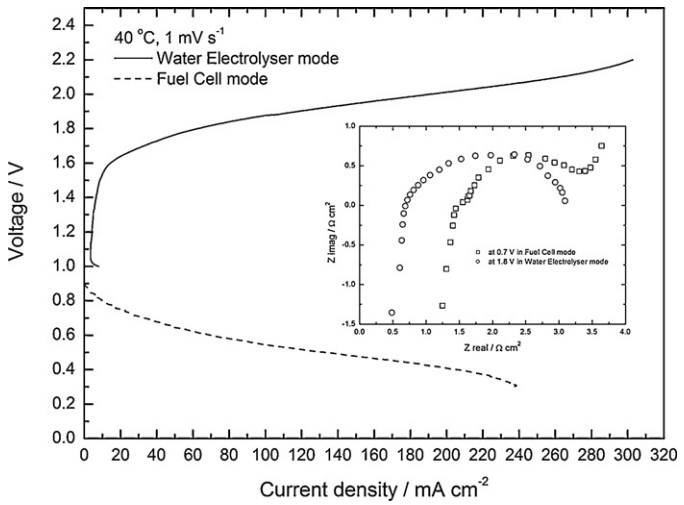

Fig. 9. Polarization curves of this regenerative fuel cell in (A) water electrolyser mode and (B) fuel cell mode, insert figure is impedance spectroscopy at 1.8 V in water electrolyser mode and at 0.7 V in fuel cell mode.

3.5. Regenerative fuel cell performances

Fig. 8(A) shows cross-section of a typical MEA prepared with CCM methods, as described in Section 2.2. Two porous coatings on the upper side and bottom side are respectively the oxygen electrode layer and hydrogen electrode layer. The CCM method may effectively reduce MEA resistance caused by membrane/catalyst–layer interface. As an example, the $Cu_{0.6}Mn_{0.3}Co_{2.1}O_4$ catalyst was adopted in the oxygen electrode layers of this study. Once the MEA was changed to OH^- form, it must be stored in N_2 gas to prevent CO_2 from air contaminating the hydroxyls. The MEA was quickly in the testing system, followed by quick filling the chambers (shown in Fig. 1) with deionized water.

Fig. 9 shows the polarization curves of this regenerative fuel cell in (A) water electrolyser mode and (B) fuel cell mode. In water electrolyser mode, in which deionized water in the chambers were being consumed and oxygen and hydrogen gases were generating on each side, the onset voltage for water electrolysis was about 1.55 V, which is in accordance with the OER catalytic activities of $Cu_{0.6}Mn_{0.3}Co_{2.1}O_4$ shown in Fig. 7. The current density performance of this MEA is several times smaller than that of conventional alkaline water electrolysers [13], which may be mainly due to its large electrolytic resistance (about 0.75 $\Omega\,cm^2$ as measured by EIS, see Fig. 9 inset). In the fuel cell mode, the electrolytic resistance of MEA was even larger than in water electrolyser mode (about 1.45 $\Omega\,cm^2$ from EIS), which might be a result of conductivity variation due to changes in humidity. Large MEA resistance leaded to its poor current density performances in fuel cell mode, yielding a peak power density of about 80 mW cm^{-2}. Since this MEA operates without electrolytes such as KOH, ionic conduction through the MEA mainly relies on the hydroxyl groups of the membrane and the ionomer in catalyst layers. Therefore, efforts shall be made to further improve hydroxyl conductivity in future studies. The current density performances of Nafion-based Pt—IrO_2 electrodes [4] are several times higher than the results of this MEA. However, a possible way to overcome this difference is using larger electrode areas of MEA, which might be feasible since the prices of this non-precious metal are much cheaper than those precious metals. At 100 mA cm^{-2} the voltages of fuel cell mode and electrolyser mode were respectively 0.58 V and 1.82 V. If the energy input and output both operate with a current density of 100 mA cm^{-2}, the fuel cell to electrolyser voltage ration is about 31.87%, which may be taken as an indicator of good efficiency of this energy device.

4. Conclusions

A non-precious metal bifunctional oxygen electrode was successfully prepared and applied in a conceptual rechargeable H_2—O_2 battery (or a regenerative fuel cell) using AAEMs. The $Cu_xMn_{0.9-x}Co_{2.1}O_4$ electrode used in this work exhibited promising ORR activity, similar to Pt/C electrode, with only 50 mV less positive in half wave potentials and OER catalytic activity better than Pt/C, with 100 mV more negative onset potentials. Current density performances of this MEA were reasonable although were affected by large electrolytic resistance, due in part to the use of deionized water and not alkaline electrolyte, in the system. However, this $Cu_xMn_{0.9-x}Co_{2.1}O_4$ catalyst is an initial example of the bifunctional catalysts based on spinel cobaltite which will be further studied concerning their surface properties, and be improved in terms of species and contents of doping metals. Improvements in conductivity of the membrane and ionomer used in the catalyst layers will be incorporated in future studies. The stability of this regenerative fuel cell will also be investigated. Overall utilization of non-precious metal bifunctional oxygen electrode in regenerative fuel cell may possibly make it a potentially competitive energy conversion device.

Acknowledgements

The authors sincerely acknowledge Dr. J.A. Horsfall and Dr. C. Williams from Department of Materials & Medical Sciences, Cranfield University, U.K., for providing the alkaline anion exchange membranes adopted in this study. This research is supported by EPSRC projects No. EP/G030995/1, EP/F035764/1, and EP/H007962/1.

References

[1] J. Ahn, R. Holze, J. Appl. Electrochem. 22 (1992) 1167–1174.
[2] Y. Gorlin, T.F. Jaramillo, J. Am. Chem. Soc. 132 (2010) 13612–13614.
[3] M. Armand, J.M. Tarascon, Nature 451 (2008) 652–657.
[4] T. Ioroi, N. Kitazawa, K. Yasuda, Y. Yamamoto, H. Takenaka, J. Electrochem. Soc. 147 (2000) 2018–2022.
[5] G. Chen, S.R. Bare, T.E. Mallouk, J. Electrochem. Soc. 149 (2002) A1092–A1099.
[6] E.H. Yu, K. Scott, J. Power Sources 137 (2004) 248–256.
[7] M. Hamdani, R.N. Singh, P. Chartier, Int. J. Electrochem. Sci. 5 (2010) 556–577.
[8] E. Rios, J.L. Gautier, G. Poillerat, P. Chartier, Electrochim. Acta 44 (1998) 1491–1497.
[9] T. Ohsaka, L. Mao, K. Arihara, T. Sotomura, Electrochem. Commun. 6 (2004) 273–277.
[10] F. Cheng, J. Shen, B. Peng, Y. Pan, Z. Tao, J. Chen, Nat. Chem. 3 (2011) 79–84.
[11] M. De Koninck, S.C. Poirier, B. Marsan, J. Electrochem. Soc. 154 (2007) A381–A388.
[12] M. De Koninck, B. Marsan, Electrochim. Acta 53 (2008) 7012–7021.
[13] X. Wu, K. Scott, J. Mater. Chem. 21 (2011) 12344–12351.
[14] M. Mamlouk, S.M.S. Kumar, P. Gouerec, K. Scott, J. Power Sources 196 (2011) 7594–7600.
[15] W. Xu, K. Scott, Int. J. Hydrogen Energy 35 (2010) 12029–12037.
[16] M. Sugawara, M. Ohno, K. Matsuki, J. Mater. Chem. 7 (1997) 833–836.